Rayleigh-Taylor Instability Experiments with Precise and Arbitrary Control of the Initial Interface Shape

Zhibin Huang, Antonio De Luca, Timothy J. Atherton, Matthew Bird, and Charles Rosenblatt
Department of Physics, Case Western Reserve University, Cleveland, Ohio 44106-7079 USA

Pierre Carlès
Institut Jean le Rond d'Alembert, Université Paris 6/CNRS, Case 162, 4 Place Jussieu, 75252 Paris Cedex 05, France
(Received 27 March 2007; published 15 November 2007)

In a Rayleigh-Taylor instability a dense fluid sits metastably atop a less dense fluid, a configuration that can be stabilized using a magnetic field gradient when one fluid is highly paramagnetic. On switching off the magnetic field, the instability occurs as the dense fluid falls under gravity. By affixing appropriately shaped magnetically permeable wires to the outside of the cell, one may impose arbitrarily chosen and well-controlled initial perturbations on the interface. This technique is used to examine both the linear and nonlinear growth regimes for which the perturbation amplitudes, growth rates, and nonlinear growth coefficients are obtained.

DOI: 10.1103/PhysRevLett.99.204502 PACS numbers: 47.20.Ma, 47.50.Ef

The general Rayleigh-Taylor (RT) instability occurs when a density gradient is subjected to an acceleration by an antiparallel pressure gradient in the presence of perturbations, i.e., when $\nabla P \cdot \nabla \rho < 0$ [1–3], where P is the pressure and ρ is the mass density. This occurs, for example, when a dense fluid is placed above a less dense fluid in the presence of gravity and then falls when the interface is perturbed. The RT instability develops in three stages, beginning with an exponential growth in which each perturbation mode develops independently and is well described by linear stability theory [3]. When the mode amplitude becomes comparable to its wavelength, nonlinearities cause the growth rate to decline [4–6], with bubbles of less dense fluid rising parallel to $\nabla \rho$ and separated by narrower spikes of denser fluid traveling in the opposite direction. Finally, the now large amplitude modes interact strongly, the scale of the dominant structures increases, fluid interpenetration becomes turbulent, and memory of the initial perturbations fades or is lost [6–9]. It is these last two stages that receive the overwhelming bulk of attention, as there are significant inconsistencies among theory, simulation, and experiment [10]. This is due in large part to poorly defined initial conditions in experiments, particularly the presence of uncontrolled long-wavelength perturbations. To date experiments have been based mainly on physical motion of the cell [5,7,10–15]. These protocols suffer from jitter and not-well-controlled initial conditions and tend to be poorly suited for establishing initial interface perturbations that involve a specific single mode or spectrum of modes [13,16].

In this Letter we demonstrate how an extension of our magnetic levitation technique [17,18] enables us to fine-tune the initial conditions. We accomplish this by affixing precisely shaped magnetically permeable materials to the outside of the fluid cell, which perturb the magnetic force and thereby the shape of the interface. On turning off the magnetic field, the total magnetic force disappears, leading to a purely gravity-driven RT instability with precisely controlled initial conditions. As a first application, we measure the amplitude of the initial interface perturbation and its growth due to an applied single-mode perturbation as a function of the amplitude of a pair of sinusoidally shaped magnetically permeable wires.

In our experiments fluid 1 is a moderately strong paramagnetic mixture of water, 58.6 wt. % $MnCl_2 \cdot 4H_2O$, approximately 1 wt. % surfactant octa(ethylene glycol) dodecyl ether ("$C_{12}E_8$") to reduce surface tension, and a small amount of rhodamine 6G dye; fluid 2 is weakly diamagnetic hexadecane, which is immiscible with fluid 1 and of nearly the same refractive index. The interfacial tension $\gamma = (2.6 \pm 0.3)$ erg cm^{-2}, as determined by the pendant drop technique, and wetting properties are such that the meniscus is virtually absent. When placed in a cell, the lighter hexadecane ($\rho_2 = 0.773$ g cm^{-3}) ordinarily sits atop the heavier paramagnetic mixture (density $\rho_1 = 1.394$ g cm^{-3}), where the Atwood number $A \equiv (\rho_1 - \rho_2)/(\rho_1 + \rho_2) = 0.29$. However, in the presence of a vertical magnetic field gradient $\nabla(H^2)$ [$\sim 2.0 \times 10^7$ G^2 cm^{-1} at the interface], the denser fluid 1 resides above the less dense fluid 2 when $|\frac{1}{2}\chi_1 \nabla(H^2)| > |(\rho_1 - \rho_2)g|$; see Fig. 1. Here χ_1 is the (positive) magnetic susceptibility of fluid 1 and the susceptibility of fluid 2 is negligible. On switching off the magnetic force, the layering becomes unstable in the presence of small, random perturbations—the large, controlled interfacial perturbations have not yet been applied—and the denser fluid 1 falls to the bottom of the container under uniform gravity. Figure 2(a) [where (a) refers to the column] shows how the instability develops as a function of time for these fluids, with the initial observable growth being that of the fastest growing mode. In this experiment the cell is constructed of 0.2 cm thick glass, is 15 cm in height, 7 cm in width

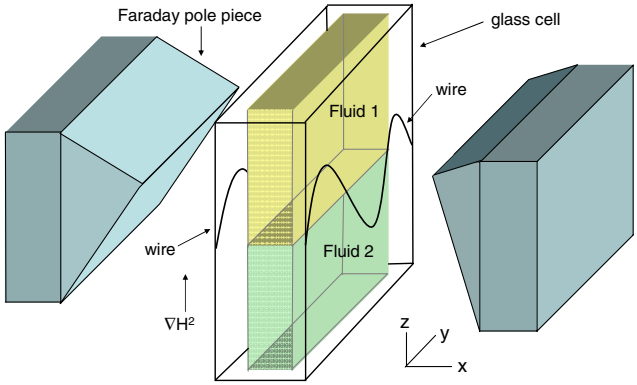

FIG. 1 (color online). Cartoon of experimental setup. Note that wires are attached to the outside of the cell and that the x axis view is expanded for clarity. The arrow indicating the direction of $\nabla(H^2)$ applies only in the absence of the wires.

(spanwise, along the y axis), and $d = 0.3$ cm thick (i.e., the cell gap along the x axis), and has no observable meniscus [Fig. 2(a), row i]. Because the characteristic time for viscous diffusion across the cell [18] $t_v \sim d^2\rho/\pi\bar{\eta} \sim$ 0.5 s, where $\bar{\eta} \sim 5$ cP is the mean viscosity, the system can be considered to be in the purely 2D RT regime for time $t \lesssim t_v$. Using the technique of planar laser induced fluorescence [19], the cell is illuminated from above with a $\sim$0.1 cm thick "sheet" of light, created by passing a Nd:YaG laser beam at 532 nm through a cylindrical lens. The light sheet passes through the midplane of the cell, causing the dye in fluid 1 to fluoresce. Videos of the lower portion of the cell are collected at 60 frames per second using a CCD camera. (Simultaneous imaging of both upper and lower portions of the cell will become possible in the future with the addition of a second synchronized camera). On switching off the magnet, the instability passes first through the linear regime [Fig. 2(a), row ii] with a wavelength $\lambda^* = (0.69 \pm 0.05)$ cm for the fastest growing mode (denoted by an asterisk), consistent with the prediction of $\lambda^* = 0.71$ cm from linear stability theory (LST) [3]. (We note that the measured λ^* values also are nearly identical for cells of other thicknesses, *viz.*, $d = 0.2$ and $d = 0.4$ cm.) Because of the small wavelength, video frames at early times have an insufficient number of pixels to resolve properly the initial growth rate σ^*, which LST predicts to be 33.5 s^{-1}. Using several well-resolved images at later times for which $h_k/\lambda^* \gtrsim 0.15$, where h_k is the perturbation amplitude, we experimentally find $\sigma^* = (24 \pm 0.5)$ s^{-1}; as expected, this is smaller than the LST prediction because the instability is already transitioning from the linear to the nonlinear regime, as seen in Fig. 2(a), rows iii through vi.

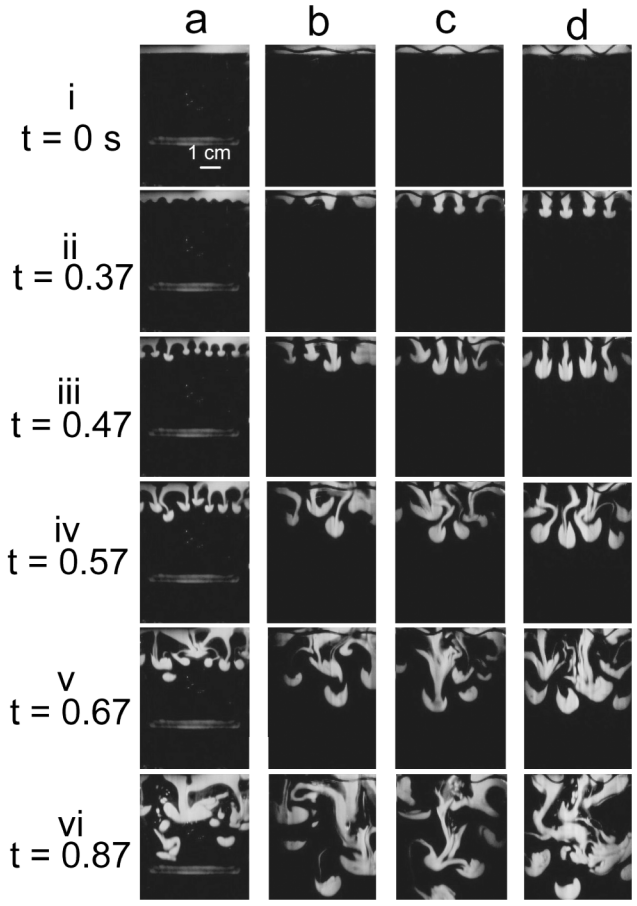

FIG. 2. Images of spike growth vs time in seconds, where $t = 0$ is the time at which the magnet current first begins to decrease. Column (a): no wire; (b)–(d): wires of amplitude $A_w = 0.1$, 0.2, and 0.3 cm, respectively. The scale is shown in the upper left panel.

Aside from physically agitating the cell to create standing waves [20]—a technique that severely limits the range of initial conditions and creates unwanted jitter—there is no viable extant method for establishing an arbitrary and controlled initial interface shape. Here we show that the interface shape can be manipulated by perturbing the magnetic field's spatial profile. We use several pairs of T-304 cold-worked stainless steel wires (diameter = 0.088 cm) bent into a sinusoidal shape with a period of 2.25 cm and amplitudes $A_w = 0.10$ [Fig. 2(b)], 0.15, 0.20 [Fig. 2(c)], 0.25, and 0.30 cm [Fig. 2(d)]. The wire's relative magnetic permeability $\mu = (2.6 \pm 0.3)$, as measured by balancing the upward magnetic force against downward gravity. Each pair of wires, painted black to reduce spurious light, is affixed to the outside of the cell's two faces; see Fig. 1. The front wires can be seen as a silhouette in each image in Figs. 2(b)–2(d); the rear wires are obscured and not easily visible. We emphasize that all aspects of the experiments shown in Fig. 2, including both the fluids and the cell, are identical, except for the addition of the wires in Figs. 2(b)–2(d). [Note that the wires are placed so that the fluid interface is at the wires' midpoint along z. The *apparent* vertical displacement in Fig. 2 is an illusion due to parallax.] On application of an external field the fluid interface is perturbed very slightly by the spanwise inhomogeneous magnetic force induced by the wires [Figs. 2(b), row i, 2(c), row i, and 2(d), row i], where the period of the interface instability $\lambda = 1.12$ cm is exactly one-half that of the

TABLE I. Interface perturbation amplitude h_{k0}, terminal velocity, and growth coefficient for different wire amplitudes A_w.

A_w (cm)	No wire	0.1	0.15	0.2	0.25	0.3
$10^4 \times h_{k0}$ (cm)	0.043 ± 0.008	0.4 ± 0.1	0.9 ± 0.2	1.6 ± 0.4	3.9 ± 0.9	6 ± 1
$(dh_k/dt)_t$ (cm s^{-1})	8 ± 0.5	11 ± 1	11 ± 1	10 ± 2	10 ± 1	11 ± 1
α_s	0.065 ± 0.01	0.06 ± 0.02	0.07 ± 0.01	0.06 ± 0.02	0.06 ± 0.01	0.07 ± 0.02

wires. λ can be understood by noting that, even at the cost of surface and buoyancy energies, the magnetic fluid accumulates near regions where the wire's projection crosses the interface, resulting in a perturbation of the interface with half the wire's period. Although too small to image, the amplitude h_{k0} of the initial perturbation at wave vector k can be estimated. The amplitude h_k for the early growth can be derived from the equation $d^2h_k/dt^2 - \sigma^2 h_k = 0$, where σ is approximately proportional to $A^{1/2}$ [3]. However, because the magnetic force decays exponentially with a time constant $\tau_m \sim 0.065$ s, the *effective* Atwood number $\sim A(1 - e^{-t/\tau_m})$. Thus, $d^2h_k/dt^2 - \sigma^2(1 - e^{-t/\tau_m})h_k = 0$. The solution $h_k = h_{k0}J_{-\beta}(\beta e^{-t/2\tau_m})/J_{-\beta}(\beta)$, where $J_{-\beta}$ is a Bessel function of the first kind of order $-\beta$ and $\beta = 2\sigma\tau_m$, is equal to $h_{k0}\exp(\sigma t)$ in the limit $\tau_m \to 0$. Fitting h_k to the two earliest resolvable interface amplitudes $h_k(t)$ (such that $h_k k \sim 0.5$) for each wire amplitude A_w, along with the LST values $\sigma = 33.0$ s^{-1} (cells with wires, $k = 5.6$ cm^{-1}), we determine h_{k0} (Table I) and the dimensionless quantity kh_{k0} (inset in Fig. 3). These values are considerably larger than those that occur without the perturbing wires (Table I), where we use the LST value $\sigma^* = 33.5$ s^{-1} (cell without wires, $k^* = 9.1$ cm^{-1}). Additionally, the data indicate that h_{k0} increases smoothly with A_w. When the field is switched off, Fig. 2(b), rows ii through vi, Fig. 2(c), rows ii through vi, and Fig. 2(d), rows ii through vi show the evolution of the perturbations. (In fact, data were collected for a total time $t \sim 30/\sigma^*$ s before the spikes reached the bottom of the cell.) Several features are apparent. First, as noted above, the wavelength of the instability is half that of the wire. Second, spikes arising from initially larger amplitude perturbations of the fluid interface in Fig. 2 grow to correspondingly longer lengths (i.e., larger h_k) before the instability evolves into the late time regime. This behavior occurs because of the larger initial amplitudes h_{k0}: the imposed mode can grow significantly before interaction with other modes becomes important. Figure 4(a) shows the advance h_k vs time of the spike front for the $A_w = 0.3$ cm amplitude wire [Fig. 2(d)], as defined by the maximum extent to which at least 5% of the denser fluid has fallen. Figure 4(b) shows its velocity dh_k/dt, and Fig. 4(c) shows the instantaneous growth coefficient α_s, defined as $(dh_k/dt)^2/4Agh_k$, where g is the gravitational acceleration [21,22]. (Values for α_s for all runs are collected in Table I.) α_s and its bubble counterpart a_b have been the subject of intense interest [10,23], as there are significant discrepancies between experiments, which have been plagued by not-well-controlled initial conditions, and calculations, which depend critically upon the initial perturbation spectrum and often are smaller than experimental values. For example, calculated values for the growth rate are $\sim$0.03 [23,24], 0.025 to 0.06 [25], 0.033 to 0.06 [22], and 0.06 [26]. We note from Fig. 4(c) that $\alpha_s \sim (0.07 \pm 0.02)$ during the self-similar growth period $t = 0.3$ to $t = 0.45$ s, after which it decays as the velocity has reached a terminal value $(dh_k/dt)_t \sim 11$ cm s^{-1} [Fig. 2(d), row iii]. Although we expect—and observe—a terminal velocity for small A

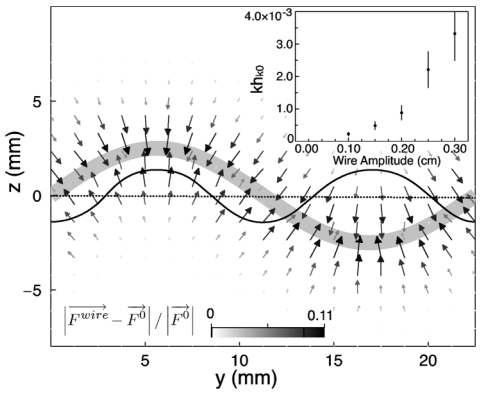

FIG. 3. Main figure: $|\vec{F}^{\text{wire}} - \vec{F}^0|/|\vec{F}^0|$ in the midplane of the cell for $A_w = 0.25$ cm. The wide gray curve is the projection of wire into the midplane, the dotted line is the fluid interface at $t = 0$, and the solid curve is the actual fluid interface measured at $t = 0.265$ s. The force, which affects fluid 1 due to its large χ_1, is largest near the wire's crossing points and results in a collection of fluid 1 at the crossing points. Inset: Dimensionless interface perturbation amplitude kh_{k0} vs wire amplitude A_w.

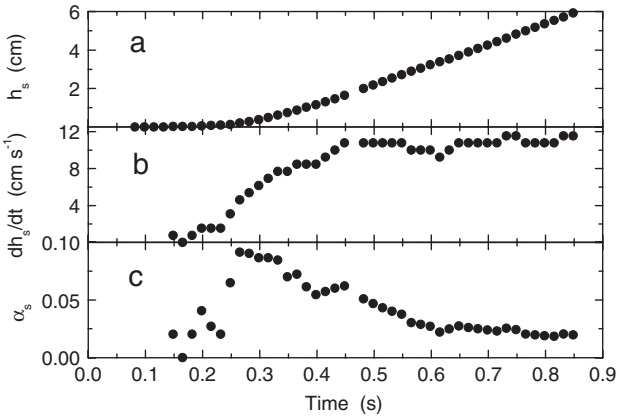

FIG. 4. Growth data vs time for a cell with a wire of amplitude $A_w = 0.3$ cm. (a) The position of the front, (b) the velocity of the front, and (c) the instantaneous growth coefficient α_s.

when only a single mode is present [14,27], we believe that the observed terminal velocity's origin lies elsewhere. That the crossover from self-similar growth to terminal velocity always occurs in the neighborhood of $t \sim 0.5$ s, which corresponds to the diffusion time t_ν for the surface vorticity layer, suggests that the terminal velocity is due in part to the instability's transitioning from the 2D RT to the Hele-Shaw regime [18]. We emphasize that the initial linear growth regime and most of the subsequent self-similar growth regime, both taking place before vorticity has reached the midplane of the cell, should thus be very little influenced by friction at the glass walls. It also has been suggested that fluctuations result in a coarsening of the spikes and droplet break off, leading to Stokes-like frictional flow with a terminal velocity [26].

We now calculate the static force on the fluids in the presence of the wires. In the absence of current a scalar magnetic potential φ may be introduced into Laplace's equation $\nabla \cdot (\mu \nabla \varphi) = 0$, where $\vec{H} = -\nabla\varphi$. A commercial finite-element package, FLEXPDE, is used on a computational domain of $3.0 \times 2.25 \times 4.0$ cm, with periodic boundary conditions. In the model the wires are sinusoidally shaped with $A_w = 0.25$ cm, period 2.25 cm, relative permeability $\mu = 2.6$, and square cross section, such that the wires' cross-sectional area is equal to that in the experiment. Dirichlet conditions are applied at the pole pieces. The total magnetic force $\vec{F}^{\text{wire}}[\propto (\vec{H} \cdot \nabla)\vec{H}]$ with the wires present minus the force $\vec{F}^0$ in the absence of the wires, scaled by $\vec{F}^0$, at the cell's midplane is plotted in Fig. 3; also shown is the experimental interface at $t = 0.265$ s. It is clear that the wires produce a force on paramagnetic fluid 1 that is directed toward the wire's crossing points with the interface. Thus the overall energy, including magnetic, gravitational, and surface tension, can be reduced if the paramagnetic (upper) fluid collects near the wire-fluid interface crossings, lowering the interface near the crossings and raising it near the wires' extrema. For small wire amplitude A_w the shape of the interface is very nearly a single sinusoid, as seen in Fig. 3. With increasing A_w, however, contributions from higher harmonics of k begin to emerge, suggesting that h_{k0} can be increased more efficaciously by increasing μ or the wire diameter.

To summarize, we have studied the growth of an imposed single-mode perturbation. One also can create an arbitrary spectrum of initial perturbation modes, requiring the solution of the inverse problem in which the appropriate magnet current and wire parameters need to be determined to achieve the desired initial perturbation. Besides demonstrating a powerful technique for RT experiments with arbitrary initial conditions, this work has yielded a precise measurement of the growth coefficient α_s, independent of wire amplitude, for a precise set of experimental conditions: a moderately large Atwood number ($A = 0.29$) and a jitter-free single-mode initial perturbation, two elements that would have been difficult to achieve by other means. Clearly, the ability to manipulate the initial interface shape facilitates many heretofore inaccessible investigations involving controlled initial conditions.

We thank K. Kadau, J. L. Barber, B. J. Alder, Xi Shan, P. L. Taylor, and D. Kang for useful discussions. This work was funded by NASA and the International Relations Departments of Université Pierre et Marie Curie (Paris 6) and CNRS, under the form of a PICS grant.

[1] Lord Rayleigh, Proc. London Math. Soc. **s1-14**, 170 (1882).
[2] G. I. Taylor, Proc. R. Soc. A **201**, 192 (1950).
[3] S. Chandrasekhar, *Hydrodynamic and Hydromagnetic Instability* (Clarendon, Oxford, 1961).
[4] D. J. Lewis, Proc. R. Soc. A **202**, 81 (1950).
[5] H. W. Emmons, C. T. Chang, and B. C. Watson, J. Fluid Mech. **7**, 177 (1960).
[6] U. Alon *et al.*, Phys. Rev. Lett. **74**, 534 (1995).
[7] K. I. Read, Physica (Amsterdam) **12D**, 45 (1984).
[8] D. L. Youngs, Physica (Amsterdam) **12D**, 32 (1984).
[9] S. W. Haan, Phys. Fluids B **3**, 2349 (1991).
[10] G. Dimonte and M. Schneider, Phys. Rev. E **54**, 3740 (1996).
[11] P. F. Linden and J. M. Redondo, Phys. Fluids A **3**, 1269 (1991).
[12] M. J. Andrews and D. B. Spalding, Phys. Fluids A **2**, 922 (1990).
[13] R. L. Cole and R. S. Tankin, Phys. Fluids **16**, 1810 (1973).
[14] J. T. Waddell, C. E. Niederhaus, and J. W. Jacobs, Phys. Fluids **13**, 1263 (2001).
[15] M. B. Schneider, G. Dimonte, and B. Remington, Phys. Rev. Lett. **80**, 3507 (1998).
[16] R. Popil and F. L. Curzon, Rev. Sci. Instrum. **50**, 1291 (1979).
[17] M. P. Mahajan *et al.*, Phys. Fluids **10**, 2208 (1998).
[18] P. Carlès *et al.*, Phys. Rev. Lett. **96**, 104501 (2006).
[19] G. Kychakoff *et al.*, Science **224**, 382 (1984).
[20] C. E. Niederhaus and J. W. Jacobs, J. Fluid Mech. **485**, 243 (2003).
[21] A. W. Cook, W. Cabot, and P. L. Miller, J. Fluid Mech. **511**, 333 (2004).
[22] J. R. Ristorcelli and T. T. Clark, J. Fluid Mech. **507**, 213 (2004).
[23] P. Ramaprabhu, G. Dimonte, and M. J. Andrews, J. Fluid Mech. **536** (2005).
[24] G. Dimonte *et al.*, Phys. Fluids **16**, 1668 (2004).
[25] G. Dimonte, Phys. Rev. E **69**, 056305 (2004).
[26] K. Kadau *et al.*, Proc. Natl. Acad. Sci. U.S.A. **104**, 7741 (2007).
[27] V. N. Goncharov, Phys. Rev. Lett. **88**, 134502 (2002).